Proceedings of the Sixth International Conference on
Railway Technology: Research, Development and Maintenance
Edited by: J. Pombo
Civil-Comp Conferences, Volume 7, Paper 3.12
Civil-Comp Press, Edinburgh, United Kingdom, 2024
ISSN: 2753-3239, doi: 10.4203/ccc.7.3.12

Study on Mathematical Model Construction of Typical Gorge Wind Field

G. Yang, J. Cheng, D. Guo and Z. Sun

**Key Laboratory for Mechanics in Fluid Solid Coupling Systems,
Institute of Mechanics, Chinese Academy of Sciences
Beijing, China**

Abstract

Wind conditions in gorges have a significant impact on the safe operation of high-speed trains, yet traditional numerical simulations rely on oversimplified wind models that fail to capture the complex wind speed distribution resulting from the boundary layer on the mountain surface. To address this, a three-dimensional, incompressible, steady calculation method is used to study wind field characteristics in a typical gorge. We propose a two-dimensional mathematical model to study the effects of gorge width on model parameters, including wind speed growth indices in the height and horizontal directions, respectively. Our results demonstrate that the thickness of the mountain boundary layer can reach a maximum of approximately 30m. Notably, we observe differences in wind speed growth indices parameters at the entrance and midway through the gorge, while the boundary layer thickness remains constant with increasing gorge width. Our findings provide more accurate boundary conditions for numerical simulations of high-speed train operation in gorge wind conditions.

Keywords: wind field characteristics, mathematical model, roughness, numerical simulation, wind speed fitting, boundary layer thickness.

1 Introduction

Trains operating in mountainous regions with precarious gorges must contend with more complex and unpredictable gorge wind loads due to the mountainous terrain's complicated topography and abundance of gorges. In addition to serving as the foundation for bridge wind resistance design [1], the research of gorge wind field characteristics also serves as a guarantee for the safe operation of trains. The airflow will speed up via the

gorge entrance as the wind moves from the open area to the gorge area where two mountains are facing one other, creating the nonuniform gorge wind [2]. The reduced riding comfort of the trains caused by the gorge wind raises the safety risk. Especially when the train enters and exits the tunnel frequently in a short time under gorge wind loads. The flow around the train is complex, the aerodynamic loads distributed on each section of the car body are different and mutable, and this causes the train to run unsteadily due to complex aerodynamic effects caused by sudden changes in the flow field, even resulting in major safety accidents like derailment and overturning [3]. While the conventional study of train operation in a crosswind is not accurate enough for the setting of wind field boundary conditions, it is imperative to explore a more realistic gorge wind model to provide more exact boundary conditions for the numerical simulation of train operations in the gorge area.

To overcome limitations in wind field measurement and region-specific numerical simulations, this study develops mathematical models to describe wind fields in gorges for high-speed train operations over bridges and tunnels. a typical gorge calculation model is constructed to evaluate wind field characteristics, and a gorge wind field model is developed and compared to other models, leading to more precise boundary conditions and theoretical recommendations for safe high-speed train operation in mountainous regions.

2 Calculation method and model

2.1 Governing equations

The gorge wind field was computed using the commercial software STAR-CCM+, and the three-dimensional, incompressible, steady N-S equation was solved.

2.2 Wall roughness

In numerical simulations of complex terrain, the velocity distribution at the ground surface is greatly influenced by surface roughness. Surface roughness can be described in two ways, with engineers most often using the roughness length y_0, which is the height from the ground surface to the point in the near-ground layer where wind speed is zero [4]. The second way to express surface roughness is through the physical roughness height r, which corresponds to the equivalent sand grain height in circular tube turbulence experiments. according to literature [5], the roughness length is 1m.

This paper employs the wall function to calculate the velocity around the wall, dividing it into a viscous bottom layer, a logarithmic layer, and a turbulent layer. The first grid layer is set to be within the logarithmic layer by default. Equation (1) shows the velocity distribution in the logarithmic layer.

$$\frac{u}{u^*} = \frac{1}{\kappa}\ln\left(E' \frac{yu^*}{\nu}\right) \tag{1}$$

$$E' = \frac{E}{f} \tag{2}$$

Where u is the velocity, κ is the von Karman constant, which takes the value of 0.42, u^* is the reference velocity, which is derived from the turbulence volume of the turbulence model, v is the kinematic viscosity coefficient, y is the distance from the centre of the grid to the wall, E is the default constant, which takes the value of 9, and

f is the roughness function.

The dimensionless quantity is defined as $R^+ = ru^* / \upsilon$ and the roughness function f is a segmented function [6].

When $R^+ \le \mathrm{R}^+_{\mathrm{smooth}}$,

$$f = 1 \tag{3}$$

When $\mathrm{R}^+_{\mathrm{smooth}} < R^+ \le \mathrm{R}^+_{\mathrm{rough}}$,

$$f = \left[\mathrm{B}\left(\frac{R^+ - \mathrm{R}^+_{\mathrm{smooth}}}{\mathrm{R}^+_{\mathrm{rough}} - \mathrm{R}^+_{\mathrm{smooth}}} \right) + \mathrm{C}R^+ \right]^a \tag{4}$$

Where the index α is defined as:

$$a = \sin\left[\frac{\pi}{2} \frac{\log\left(R^+ / \mathrm{R}^+_{\mathrm{smooth}}\right)}{\log\left(\mathrm{R}^+_{\mathrm{rough}} / \mathrm{R}^+_{\mathrm{smooth}}\right)} \right] \tag{5}$$

When $R^+ > \mathrm{R}^+_{\mathrm{rough}}$,

$$f = \mathrm{B} + \mathrm{C}R^+ \tag{6}$$

In addition, the relationship between the physical roughness height r and roughness length y_0 in Star-CCM+ is

$$r = \frac{E\mathrm{y}_0}{\mathrm{C}} \tag{7}$$

The remaining parameters in the equation are $B = 0, C = 0.253, R^+_{smooth} = 2.25, R^+_{rough} = 90$.

2.3 Computational model and domain

This paper takes the Sichuan-Tibet Railway as the background, which passes through gorges ranging in depth from hundreds to thousands of meters, the length of bridges on the Sichuan-Tibet Railway is mostly between 300m-500m, and there are many sections of the Yarlung Zangbo River valley with a typically long and straight shape, and the length is about 1km-5km. Referring to this shape characteristic, we take the isosceles triangle as the cross-section of the gorge mountain, the rounded corners are made at the top of the mountain, and the height, width, and length of the completed mountain is about 450m, 500m, and 2000m respectively, the forward part of the mountain is made by rotating the triangular cross-section, the model of the gorge is shown in Figure 1, and the characteristic length is the height h of the gorge, the dimension of the calculation domain is shown in Figure 2.

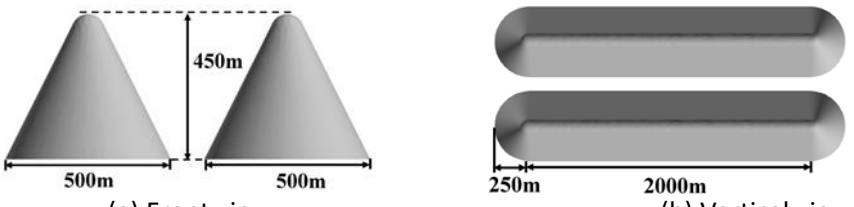

(a) Front view (b) Vertical view

Figure 1. Gorge model.

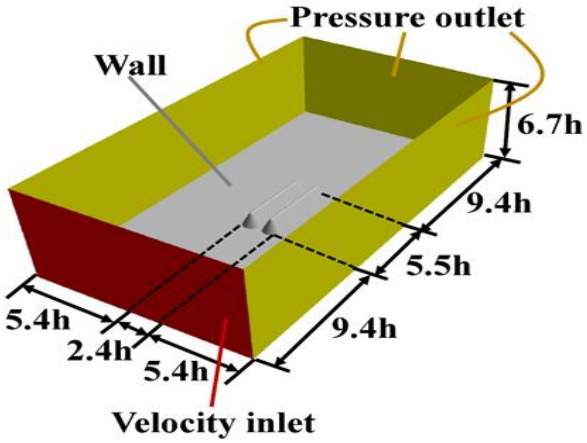

Figure 2. Schematic diagram of the calculation domain

2.4 Boundary conditions

The boundary conditions of the simulation include velocity inlet, pressure outlet, and wall boundaries, as shown in Figure 2. The velocity inlet boundary is located in front of the gorge, and the atmospheric boundary layer exponential wind model, represented by Equation (8), is applied.

$$U = \mathrm{U}_0\left(\frac{z}{\mathrm{H_g}}\right)^{\alpha} \tag{8}$$

Where U_0 is the wind speed at the gradient wind height, which is set to 30 m/s, z is the height above the ground, H_g is the gradient wind height, and α is the roughness index. According to the wind resistance design specification for highway bridges, the inlet velocity model parameters Hg set to 350 m and α set to 0.16. the top of the computational domain is set as the symmetric boundary, and the gorge mountain is used as a rough wall boundary with a roughness height of 1 m.

3 Results and discussions

3.1 Wind field characteristics

Since the lateral wind load has the most significant impact on the stability of the train, firstly, we will be discussing the y-direction velocity components. in Figure 3, we present the velocity contours of the cross-section with varying y-coordinate values. It can be observed that the airflow at the entrance of the gorge is partially accelerated towards the middle due to the obstruction of the mountain. Meanwhile, the airflow in the middle of the gorge is slower, influenced by the ground boundary layer. As a result, high winds are present on both sides, and a low wind speed zone exists in the middle of the gorge, as indicated by the black dashed boxes in the figure. As we move towards the back of the gorge, the low wind speed zone gradually expands, and after stabilization, it extends up to 250 m, which is approximately 56% of the gorge height.

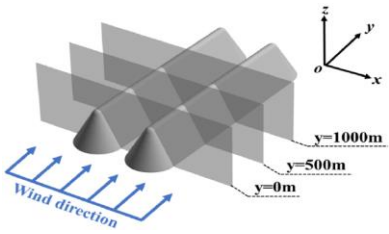

(a) Location of the sections along the y-axis

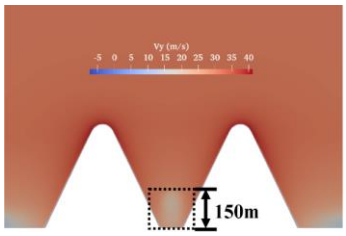

(b) Velocity contour (y=0 m)

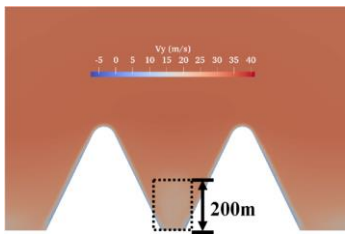

(c) Velocity contour (y=500 m)

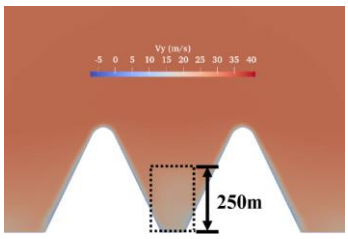

(d) Velocity contour (y=1000 m)

Figure 3. Sections location and velocity contours in y direction.

Figure 4 depicts velocity contours for three planes in the z-direction. The velocity on both sides of the mountain is bigger, especially in the area where the airflow from the front of both mountains converges and flows into the gorge. The curved shape of the mountain front reduces the flow area, leading to an increase in wind speed at the entrance of the gorge. The maximum wind speed occurs at the end of the circular arc segment, indicating the presence of a wind speed acceleration zone at the entrance. Due to the ground's obstruction to airflow, the wind speed in the middle of the wind speed acceleration zone decreases at lower heights. However, the low wind speed zone in the middle of the wind speed acceleration zone becomes less prominent as the height increases. The monitoring of wind velocity and observation of velocity contours reveal the existence of a velocity boundary layer on the mountain's surface. The wind speed at the wall is zero, and it gradually increases with the distance from the wall. In addition, the roughness height of the wall disturbs the airflow, making the velocity boundary layer on the mountain wall more distinct.

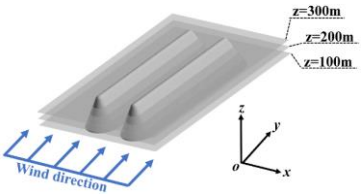

(a)Location of the sections along the z-axis

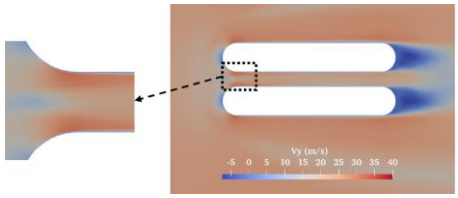

(b) Velocity contour (z=100 m)

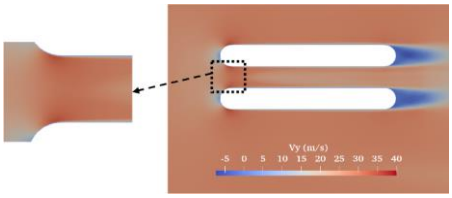

(c) Velocity contour (z=200 m)

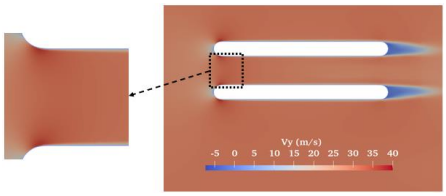

(d) Velocity contour (z=300 m)

Figure 4. Sections location and velocity contours in z-direction.

3.2 Mathematical model of gorge wind

Taking the cross-section of y=200 m as an example to study the wind field model in the

gorge. Figure 5 displays the position of the measurement spots as well as the wind speed at those points. The velocity boundary layer near the mountain wall exists, as can be seen from the distribution of wind speed at measurement points at various heights. The wind speed increases gradually from small to large with increasing horizontal distance from the wall, and the maximum value of wind speed at measurement points at various heights also rises gradually with increasing height.

(a) Position of measuring points (b) Wind speed of measuring points

Figure 5. Wind speed of measuring points.

The vertical distribution of gorge wind is described by Equation (9), which employs an expression similar to that of the exponential wind in the surface boundary layer. This equation is used to illustrate how the maximum wind speed at various heights inside the gorge is distributed. The mountain height and the wind speed at the mountain height are chosen as known characteristics.

$$U(z) = \mathrm{U_h}\left(\frac{z}{\mathrm{h}}\right)^{\alpha_1} \tag{9}$$

Analogous to the increase in wind speed with height, an exponential expression is adopted to depict the variation of wind speed in the horizontal direction. As demonstrated in Equation (10), $U_{\max}$ represents the maximum wind speed at a specific height in Equation (9). In addition, x_0 denotes the distance interval for wind speed augmentation along the horizontal direction near the mountain wall, where the wind speed is increased in the region with wall distance less than x_0. Moreover, α_2 signifies the wind speed growth index.

$$U(x) = U_{\max}\left(\frac{x}{\mathrm{x_0}}\right)^{\alpha_2} \tag{10}$$

The two-dimensional model of gorge wind can be expressed as Equation (11), where the three parameters, namely, x_0, α_1, and α_2, are determined based on the calculated wind speed.

$$U(x,z) = \mathrm{U_h}\left(\frac{z}{\mathrm{h}}\right)^{\alpha_1}\left(\frac{x}{\mathrm{x_0}}\right)^{\alpha_2} \tag{11}$$

The location of the measurement points and the corresponding wind speed are presented in Figure 6. The measurement points are separated by a horizontal distance of 50 meters from the wall. At the cross-section of y=200 m, the value of x_0 is approximately 15 m since the wind speed growth interval at different heights is primarily 15 m. It is noteworthy that 450 m corresponds to the mountain's height, and hence the boundary layer effect near the mountain's summit has diminished. Consequently, the wind speed growth interval at this height deviates from that at other heights, and the analysis for $\mathrm{x_0}$ does not take this into account.

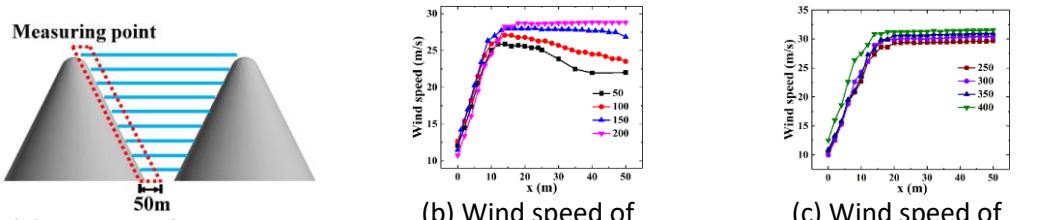

(a) Position of measuring points

(b) Wind speed of measuring points(50m-200m)

(c) Wind speed of measuring points(250m-400m)

Figure 6. Wind speed of measuring points.

After determining the wind speed growth interval near the mountain wall at x_0, we identified the maximum wind speed at each height within the x_0 interval, corresponding to the measurement location 50 meters away from the wall. Next, we fitted this data to Equation (9), where the dependent variable is U/U_h (where U_h represents the maximum wind speed at a height of 450m) and the independent variable is z/h (where z indicates the height and z = 0 at the bottom of the gorge).

(a) Wind speed on different heights

(b) Wind speed fitting

Figure 7. Parameter α_1 fitting.

The wind speed at the measurement points within 15 m from the mountain surface at different heights is fitted in the form of Equation (10) with $U/U_{\max}$ as the dependent variable (here $U_{\max}$ is the wind speed at the measurement point at 15 m in x coordinate) and x/x_0 as the independent variable (here x is the distance from the mountain wall to the measurement point), the α_2 values at heights from 100m to 400 m and the coefficients of determination are shown in Table 1.

Heights	α_2	R^2
100 m	0.29	0.94
200 m	0.41	0.98
300 m	0.47	0.98
400 m	0.37	0.97

Table 1 The fitted α_2 and the fitted determination coefficient of y=200 m cross-section.

Obviously, there is an difference between the flow state at the entrance of the gorge and the middle position of the gorge. In order to examine the difference of the parameters of the wind field model at different longitudinal depths of the gorge, the same wind field model study was conducted for the longitudinal 1/4 depth of the gorge (y=600m) and the middle depth of the gorge (y=1000m). after getting x0 from cross-sections at different y-values, the wind speed at the measured point at x_0 from the wall in the horizontal direction on the two cross-sections was fitted with Equation (9) to obtain the parameter α_1 of the wind field model, as shown in Figure 8. Comparing with α1 at the entrance of the gorge in the previous paper, the value of α_1 gradually increases as the position of the cross-section moves away from the entrance of the gorge. These results indicate that the wind speed at the gorge's entrance increases with height more quickly than it does in the middle

of the gorge because the boundary layer between the ground and mountains has less of an impact there. As the wind blows deeper into the gorge, however, the airflow becomes more and more influenced by the boundary layer, and the increase in wind speed in the height direction gradually slows down. Equation (10) was used to fit the wind speed at the measuring stations within x0 of the mountain's surface on the cross sections of y=600 m and y=1000 m. The results are displayed in Tables3 as values for α_2 and decision coefficients at various heights for the two cross-sections. As shown in the tables, the values of α_2 at the gorge's entrance are higher than the values of α_2 at its middle location at various heights, indicating that the rate of increase in wind speed at the gorge's entrance near the mountain wall is slower than at the middle location of the gorge.

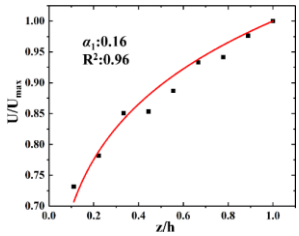

(a) Wind speed fitting (y=600 m)

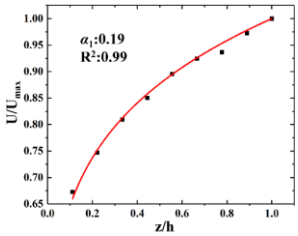

(a) Wind speed fitting (y=1000 m)

Figure 8. Comparison of parameter α_1 of different sections along the y-axis.

Heights (y=600m)	α_2	R^2
100 m	0.21	0.91
200 m	0.37	0.99
300 m	0.38	0.99
400 m	0.29	0.97

Heights (y=1000m）	α_2	R^2
100 m	0.22	0.95
200 m	0.37	0.99
300 m	0.36	0.99
400 m	0.27	0.96

Table 2 The fitted α_2 and the fitted determination coefficient.

Conclusions

This paper established a two-dimensional mathematical model of the gorge wind field by verifying the accuracy of the numerical simulation algorithm and grid through comparison with measured data. The wind field inside a typical gorge was then calculated, and the impact of the gorge's width on the model parameters was examined.

Reference

[1] Li, Y., Tang, K., Cai, x., & Liao, H. (2010). Integrated wind speed standard for long-span bridge over deep-cutting gorge. *Journal of Southwest Jiaotong University*, 45(2), 7.

[2] Niu, J., Zhou, D., Li, Z., & Yang, M. (2014). Research on aerodynamic performance of high-speed train through canyon wind zone. *Journal of the China*

Railway Society, (6), 9-14.
[3] Gao, G. (2008). Research on train operation safety under strong side wind [Doctoral dissertation, Central South University].
[4] Deng, Y., Liu, S., Yu, Z., & Zeng, X. (2010). Analysis of the impact of roughness on CFD simulation of actual terrain wind fields. Acta Energiae Solaris Sinica, 31(12), 1644–1648.
[5] Wieringa, J. (1992). Updating the davenport roughness classification. Journal of Wind Engineering & Industrial Aerodynamics, 41(1–3), 357-368.
[6] Cebeci, T., & Bradshaw, P. (1977).Momentum transfer in boundary layer. Hemisphere Pub. Corp.